*Progress In Electromagnetics Research, Vol. 121, 19–37, 2011*

# MIMO-TOPS MODE FOR HIGH-RESOLUTION ULTRA-WIDE-SWATH FULL POLARIMETRIC IMAGING

**W. Xu[1,*], P. P. Huang[2], and Y. K. Deng[1]**

[1]Department of Spaceborne Microwave Remote Sensing, Institute of Electronics, Chinese Academy of Sciences (IECAS), Beijing, China

[2]College of Information Engineering, Inner Mongolia University of Technology, Hohhot, Inner Mongolia, China

**Abstract**—The novel TOPS mode can achieve wide swath imaging coverage at the cost of impaired azimuth resolution. MIMO-SAR systems combined with multi-channel SAR signal reconstruction in azimuth and digital beamforming (DBF) on receive in elevation can overcome the inherent contradiction between swath width and azimuth resolution of conventional SAR systems. This paper derives a novel spaceborne MIMO-TOPS mode for high-resolution ultra-wide-swath full polarimetric imaging. In such an imaging scheme, different polarimetric waveforms with different elevation beam pointing directions and short time delays are transmitted in a single pulse repetition interval (PRI) by different sub-aperture antennas in azimuth. Besides improving the desired signal-to-noise ratio (SNR) and suppressing ambiguous energy in elevation, a novel DBF on receive approach including two steps is adopted to separate different echoes corresponding to sub-pulses with different polarizations. The design example of a full polarimetric MIMO-TOPS SAR system, which allows for the imaging capacity to cover an ultra wide swath of 400 km with a high azimuth resolution of 3 m, is given to validate the proposed imaging scheme.

## 1. INTRODUCTION

The Synthetic Aperture Radar (SAR) is an all-weather imaging tool that achieves fine along-track resolution by taking the advantage of radar motion to synthesize a large antenna aperture [1–6]. The TOPS (Terrain Observation by Progressive Scans) mode is a novel

*Received 2 March 2011, Accepted 10 May 2011, Scheduled 13 October 2011*

* Corresponding author: Wei Xu (iecasxuwei@gmail.com).

spaceborne wide swath SAR imaging scheme with a low azimuth resolution [7]. Moreover, it reduces the major disadvantages of conventional ScanSAR, e.g., the scalloping effect, azimuth varying ambiguity to signal ratio (ASR) and signal to noise ratio (SNR), by means of electronically steering the azimuth beam along track during the whole raw data acquisition time. The TOPS mode was firstly achieved by the TerraSAR-X satellite and chosen as the default mode of European Speace Agency (ESA)'s Sentinel-1 SAR system for its main interferometric wide swath application [8, 9]. It will also be selected as the wide swath mode for the next generation Chinese spaceborne SAR system.

However, a complete and frequent coverage of the earth with a weekly visit time and a high geometric resolution below 10 m is required for future spaceborne SAR missions [10, 11]. Burst mode is a sophisticated imaging scheme for wide swath but with a reduced azimuth resolution. To improve the impaired azimuth resolution in burst mode, several modified burst modes, e.g., elevation multibeam burst mode [12, 13] and azimuth multichannel burst mode with the technique of displaced phase center antenna (DPCA) [13, 14], are proposed in recent years. However, advanced SAR concept needs for ultra wide swath coverage with not only a high geometric resolution but also full polarimetric content [15–20]. In this regard, an innovative operation of MIMO-TOPS mode is proposed in this paper. As the mere use of simultaneously transmitting orthogonal waveforms will only disperse but not indeed suppress ambiguous energy, multidimensional waveform encoding combined with DBF on receive in elevation proposed in [21–23] is introduced in the proposed novel MIMO-TOPS mode.

This paper is arranged as follows. Section 2 describes the proposed innovative full polarimetric MIMO-TOPS mode in detail. Signal processing scheme in such an imaging mode is briefly presented in Section 3. To separate different echoes corresponding to sub-pulses with different polarizations, a modified approach of DBF on receive in elevation is proposed. The design example of a full polarimetric MIMO-TOPS mode SAR system, which achieves the imaging capacity to illuminate an ultra wide swath of 400 km with a high azimuth resolution of 3 m, is given in Section 4. Its system performances are analyzed to validate the proposed innovative imaging mode.

## 2. FULL POLARIMETRIC MIMO-TOPS MODE

Wide swath coverage with short revisit time makes conventional ScanSAR quite attractive, but the inherent drawbacks due to its special

acquisition scheme discourage its many useful applications, especially for interferometric application [7]. Progressive azimuth beam scanning is adopted in the TOPS mode, and targets with different azimuth locations are weighted by the completed and reduced azimuth antenna pattern (AAP) to avoid the major drawbacks in ScanSAR. Although imaging scheme principles in ScanSAR and TOPS mode are quite different, the obtained azimuth resolution in both modes is impaired due to the reduced target dwell time. Therefore, the impaired azimuth resolution is the major bottleneck of the novel TOPS mode.

To overcome the inherent contradiction between swath width and azimuth resolution in conventional SAR system, several techniques have been proposed [22–24] in recent years. MIMO-SAR systems, which are proposed by generalizing the information theoretic modeling of multiple-input multiple-output (MIMO) communication systems, are hotly discussed recently [22, 24]. The configuration of the proposed MIMO-SAR system in this paper with two transmitters and multiple receivers is shown in Figure 1.

In Figure 1(a), the MIMO-SAR configuration with two transmit ("Tx") sub-aperture antennas and six receive ("Rx") sub-aperture antennas are considered. Sub-pulses with different polarizations are transmitted by different sub-aperture antennas in azimuth. As a result, echoes from the same subswath corresponding to sub-pulses with different polarizations transmitted by Tx1 and Tx2 will overlap at the receivers. To separate echoes with different polarizations, different waveforms with different polarizations should be transmitted. Up

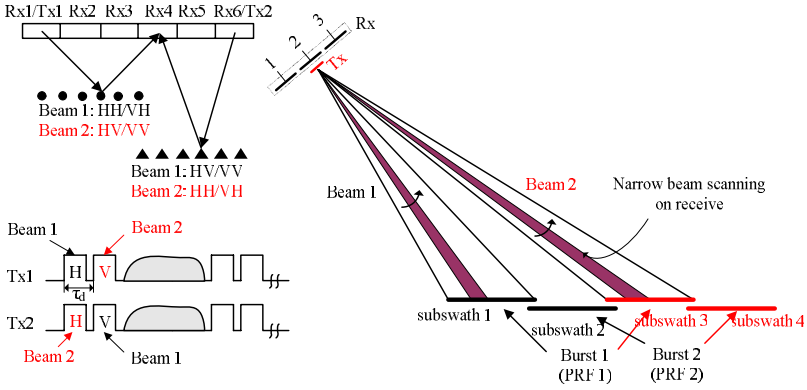


**Figure 1.** Imaging scheme of the proposed MIMO-TOPS mode. (a) In azimuth. (b) In elevation.

to now, possible waveforms can be signals from different subbands, special phase codes or short time delays [22]. Multiple subbands adopted in the MIMO-SAR systems will increase the transmitted and received bandwidth, and the complexities of such MIMO-SAR systems are seriously increased. Moreover, orthogonal waveforms with special phase codes enable a separation of the overlap at the receiver just in the case of isolated pointlike targets, as ambiguous energy is only dispersed but not indeed suppressed. Multidimensional waveform encoding in azimuth combined with DBF on receive in elevation is proposed in [22] to obtain additional spatial modulation diversities to suppress azimuth ambiguities or to increase the sensitivity to object movements, invoking the relation between the short time delay and the elevation angle in the sidelooking radar imaging geometry. DBF on receive in elevation can separate different scatter echoes from sub-pulses with different time delays. Therefore, sub-pulse with vertical polarization is transmitted by Tx1, and then sub-pulse with horizontal polarization is transmitted by Tx2 after a short time delay $\tau_d$ in a single pulse repetition interval (PRI) as shown in Figure 1(a). Afterwards, the full polarimetric contents of the scatters are obtained. It should be noted that the number of effective phase centers is only $N$ in the presented MIMO-SAR system with two transmit sub-aperture antennas and $N$ receive sub-aperture antennas.

Ultra wide swath coverage in burst mode with a reasonable antenna length requires large number of bursts, which leads the seriously reduced system performances and a coarser obtained azimuth resolution. Such problems can be mitigated by a simultaneous mapping of multiple subswaths during each burst, namely multiple elevation beam burst mode. Multiple subswaths are illuminated by a series of sub-pulses with a sequence of high gain elevation beams instead of a wide duration pulse. This operation is named intrapulse beamsteering in elevation and is an example for multidimensional waveform encoding in elevation [22]. Similar to multidimensional waveform encoding in azimuth, echoes from different subswaths will overlap at the receivers. Besides DBF on receive in elevation to separate echoes from different subswaths, a careful design of transmit antenna pattern in elevation by null-steering can further reduce the disturbance echoes from the temporal undesired sub-swath.

Therefore, multidimensional waveform encoding in both azimuth and elevation is adopted in the proposed MIMO-TOPS imaging operation as shown in Figure 1. Two transmit sub-aperture antennas and multiple receive sub-aperture antennas are adopted to obtain more phase centers, and two sub-pulses with different elevation beam pointing directions are transmitted in a single PRI by each transmit

sub-aperture. In the Figure 1, beam 1 and beam 2 are regarded as transmitting elevation beams adopted for illuminating the near subswath and the far subwath with the same burst, respectively. Taking Burst 1 with PRF 1 as an example, Tx1 transmits the first sub-pulse with horizontal polarization via the beam 1, while Tx2 transmits the sub-pulse with horizontal polarization via the beam 2 at the same time. After the time delay $\tau_d$ which is much shorter than the PRI, Tx1 transmits the second sub-pulse with vertical polarization via the beam 2, while Tx2 transmits the sub-pulse with vertical polarization via the beam 1 at the same time. After the operation of separating echoes corresponding to different subswaths and sub-pulses with different polarizations, a full polarimetric SAR system for high resolution ultra wide swath imaging is implemented.

To resolve the temporal overlap problem at the receivers, DBF on receive in elevation is required. To separate echoes from multiple sub-pulses, the height $L_r$ of the large receive antenna at least should be [22]:

$$L_r \geq \frac{2\lambda R_{far} \cdot \tan(\theta_{inc.\max})}{c\tau_d} \tag{1}$$

where $\lambda$ is the wavelength, $c$ is the speed of the light, $R_{far}$ and $\theta_{inc.\max}$ are the farthest slant range and the maximum incident angle in the imaging geometry, respectively. Moreover, DBF on receive in elevation with a large receive antenna can compensate the antenna gain of the smart transmit antenna and improve system performances especially at the edge of the subswath.

There are two major existing approaches to achieve DBF on receive in elevation. One approach adopts a number of receive sub-apeture antennas to cover the whole subswath, whose height is usually required to be equal to or smaller than the transmit antenna. Each sub-aperture receives scatter echoes in a separate channel, and each channel provides a separate input for the subsequent digital array signal processing on the ground. Taking account of multiple channels in both azimuth and elevation, too many sub-apertures lead to seriously increased the data rate and the amount of data The other approach is the novel technique of SCan-On-REceive (SCORE) [12, 14, 25]. It is possible to combine received echoes in all elevation channels into one to form a sharp and high gain receive beam, which follows the pulse echo as it travels along the ground swath. This scheme can be implemented by multiplying the fast-time variant complex coefficient vector, which can be computed previously and stored onboard based on the relation in the sidelooking SAR imaging geometry. However, this approach also brings two major drawbacks: useful information of multi-channel signals loss and gain loss from topography during pulse

chasing. The useful information of multi-channel signals in elevation can be used for interferometry mission, ambiguous energy suppression and other potential applications. Moreover, the receive gain loss due to the varying terrain height $\Delta h$ is as follows [22]:

$$\Delta G_R = \sin c \left[ \frac{L_r}{\lambda} \sin \left( \frac{\Delta h}{R \cdot \sin(\theta_{inc})} \right) \right] \tag{2}$$

where $R$ and $\theta_{inc}$ are the slant range and the incident angle, respectively. Figure 2 shows the effect of the varying mountain height during scatter echoes chasing with different receive antenna heights. It can be seen that this effect can not be neglected when the total receive antenna exceeds 1 m. In this simulation, the slant range and the incident angle are assumed as 750 km and 30°, respectively, while the carrier frequency is 9.65 GHz.

To overcome the major drawbacks of the existing DBF on receive approaches in elevation, a novel DBF approach, which makes use of the SCORE operation executed in parallel on several sub-arrays and the posterior DBF step on the ground, is proposed. In this approach, the large receive antenna in elevation is divided into several sub-array antennas whose height is larger than the transmit antenna and each receive antenna has the SCORE ability in elevation as shown in Figure 3. Therefore, the height of each sub-array antenna could be with a tolerated value to avoid the great gain loss from tomography during pulse chasing. The multiple simultaneous narrow receive beams generated by different sub-array antennas should be with the same beam steering direction during pulse chasing. Therefore, this receive approach brings another advantage: the number of input signals to form the narrow high gain steering receive beam in real time is

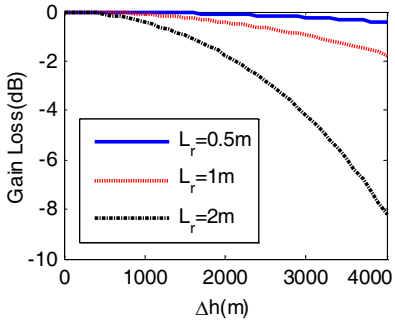


**Figure 2.** Receive gain loss during echoes chasing.

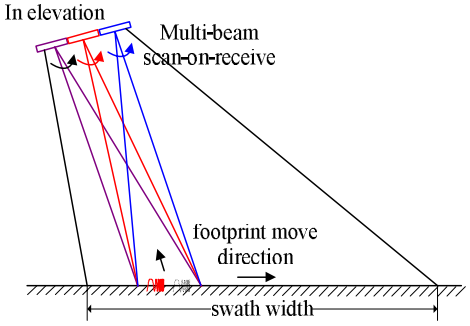


**Figure 3.** Imaging scheme of the proposed DBF on receive in elevation.

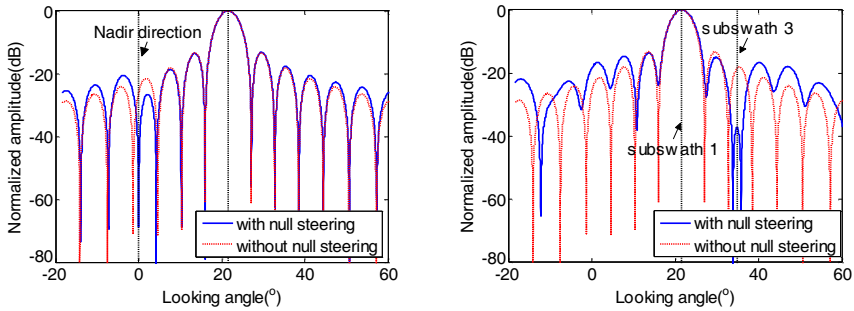


(a) Null steering for nadir echo suppression (b) Broad nulls for temporal undesired swath

**Figure 4.** ABF on transmit with null steering in elevation.

decreased, and different sub-arrays have the same DBF net during pulse chasing due to the same steering law. This will seriously reduce the complexity of the SCORE technique on board. Reflected radar echoes received by each sub-array antenna are recorded in a separated channel and then will be transmitted to the ground, and each channel provides a separate input for the subsequent DBF operation on the ground.

Aside from DBF on receive in elevation to suppress range ambiguities and nadir echoes, another possible solution can be implemented by the careful design of the transmit antenna pattern. The nadir energy could be seriously reduced by analog beamforming (ABF) on transmit in elevation with null steering as shown in Figure 4(a), and broad nulls could be used to reduce the temporal overlap at receivers due to echoes from different subswaths corresponding to different subpulses as shown in Figure 4(b). The beam pointing direction and nulls in the transmit elevation antenna pattern (EAP) are controlled by the excitation coefficients which are previously stored onboard based on the sidelooking SAR imaging geometry.

## 3. IMAGING SCHEME

In the conventional MIMO-SAR systems, imaging processors usually include three major processing steps: echoes separation corresponding to different transmitted waveforms, azimuth signal reconstruction and traditional monostatic SAR imaging processor. Similar to conventional MIMO-SAR systems, the block diagram of signal processing in the proposed MIMO-TOPS full polarimetric SAR system is shown as

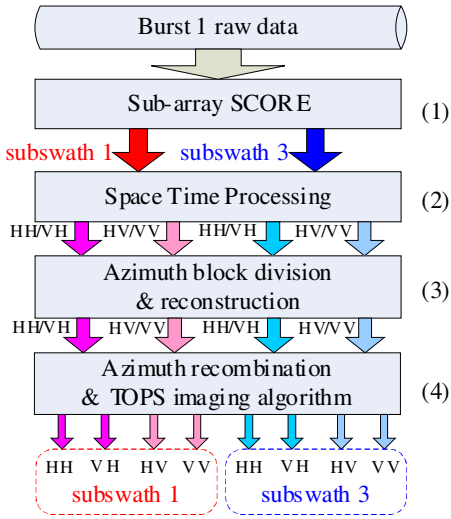


**Figure 5.** Block diagram of the imaging processor in the proposed MIMO-TOPS SAR system.

Figure 5. There are four major steps in this imaging scheme: the first DBF processing step onboard namely sub-array SCORE, the subsequent DBF step on the ground named space time processing, azimuth data preprocessing and monostatic TOPS mode SAR imaging processor.

### 3.1. Sub-array SCORE

The novel SCORE technique is first proposed in [25]. In this novel receive technique, signals received by multiple sub-apertures in elevation are combined into one to form a sharp and high gain receive beam in real time. The following chirp signal is assumed in the proposed SAR system.

$$s(\tau) = \text{rect}[\tau/\tau_p] \cdot \exp\left(j2\pi f_c \tau + j\pi k_r \tau^2\right) \tag{3}$$

where $\tau$ indicates the fast time in elevation, $\tau_p$ is the pulse duration, $f_c$ is the frequency carrier, $k_r$ is the linear frequency modulation rate. The received echo in the $k$th sub-aperture is as follows:

$$s_k(\tau) = \text{rect}\left[\frac{\tau - \tau_k}{\tau_p}\right] \cdot \exp\left[j2\pi f_c(\tau - \tau_k) + j\pi k_r(\tau - \tau_k)^2\right] \tag{4}$$

with

$$\tau_k = \tau_0 - \Delta\tau_k = \tau_0 - \frac{(k-1)}{c} \cdot d \cdot \sin(\theta_0) \tag{5}$$

where $d$ is the distance between the phase centers of two adjacent sub-aperture in elevation. $\theta_0$ indicates the actual direction of arrival (DOA) of the received echoes, $\tau_0$ denotes the time delay of the first sub-aperture in elevation, and $\tau_k$ is the time delay for the $k$th sub-aperture.

The phase weighting factor corresponding to the $k$th sub-aperture in elevation to form the sharp scanning beam is as follows:

$$w_k(\tau) = \exp\left\{-j2\pi \frac{(k-1)\cdot d}{\lambda} \cdot \sin\left[\theta(\tau)\right]\right\} \tag{6}$$

where $\theta(\tau)$ is the steer angle as a function of the fast time $\tau$. Afterwards, the final obtained signal of the $k$th sub-aperture in elevation can be expressed as follows:

$$\begin{aligned}
s_k(\tau) &= \exp\left(-j2\pi f_c \tau_0\right) \cdot \mathrm{rect}\left[\frac{\tau - (\tau_0 - \Delta\tau_k)}{\tau_p}\right] \cdot \exp\left\{j\pi k_r [\tau - (\tau_0 - \Delta\tau_k)]^2\right\} \\
&\quad \cdot \exp\left\{-j2\pi \cdot \frac{(k-1)\cdot d}{\lambda} \cdot \left[\sin\left(\theta(\tau)\right) - \sin\left(\theta_0\right)\right]\right\} \\
&\approx \exp\left(-j2\pi f_c \tau_0\right) \cdot \mathrm{rect}\left[\frac{\tau - (\tau_0 - \Delta\tau_k)}{\tau_p}\right] \exp\left\{j\pi k_r [\tau - (\tau_0 - \Delta\tau_k)]^2\right\} \\
&\quad \cdot \exp\left\{-j2\pi \cdot \frac{(k-1)\cdot d}{\lambda} \cdot \frac{\partial\theta\left(\tau_c\right)}{\partial\tau} \cdot (\tau - \tau_0)\right\} \\
&= \exp(-j2\pi f_c t_0) \cdot \mathrm{rect}\left[\frac{\tau - (\tau_0 - \Delta\tau_k)}{\tau_p}\right] \exp\left\{j\pi k_r [\tau - (\tau_0 - \Delta\tau_k)]^2\right\} \\
&\quad \cdot \exp\left\{-j2\pi \cdot \frac{(k-1)\cdot d}{\lambda} \cdot \frac{\partial\theta\left(\tau_c\right)}{\partial\tau} \cdot [\tau - (\tau_0 - \Delta\tau_k)]\right\} \\
&\quad \cdot \exp\left\{j2\pi \cdot \frac{(k-1)\cdot d}{\lambda} \cdot \frac{\partial\theta\left(\tau_c\right)}{\partial\tau} \cdot \Delta\tau_k\right\}
\end{aligned} \tag{7}$$

where $\tau_c$ is the time delay for the middle slant range in a subswath. Then, the spectrum of the received signal (7) can be expressed as follows:

$$\begin{aligned}
S_k(f) &= C_k \exp(-j2\pi f_c \tau_0) \cdot \mathrm{rect}\left[\frac{f + (k-1)\cdot f_0}{k_r \tau_p}\right] \cdot \exp\left\{-j\frac{\pi}{k_r}[f + (k-1)\cdot f_0]^2\right\} \\
&\quad \cdot \exp\left\{-j2\pi \cdot f \cdot (\tau_0 - \Delta\tau_k)\right\} \cdot \exp\left\{j2\pi \cdot \frac{(k-1)\cdot d}{\lambda} \cdot \frac{\partial\theta\left(\tau_c\right)}{\partial\tau} \cdot \Delta\tau_k\right\} \\
&= C_k \cdot \exp\left\{-j2\pi\left(f + f_c\right)\tau_0\right\} \cdot \mathrm{rect}\left[\frac{f + (k-1)\cdot f_0}{k_r \tau_p}\right] \cdot \exp\left\{-j\frac{\pi}{k_r} f^2\right\} \\
&\quad \exp\left\{j2\pi f\left(\Delta\tau_k - \frac{(k-1)}{k_r} \cdot f_0\right)\right\}
\end{aligned} \tag{8}$$

with

$$f_0 = \frac{d}{\lambda} \cdot \frac{\partial \theta(\tau_c)}{\partial \tau} \tag{9}$$

where $C_k$ is a complex constant. From (8), it can be seen that a linear phase term should be compensated via the following function.

$$H_k(f) = \exp\left\{-j2\pi f\left(\Delta\tau_k - \frac{(k-1) f_0}{k_r}\right)\right\} \tag{10}$$

This linear phase term compensation could also be implemented in the time domain via the time delay $D_k$, and it can be expressed as follows:

$$D_k = \Delta\tau_k - \frac{(k-1) f_0}{k_r} \tag{11}$$

After the modification of spectrum realized by the short time delay $D_k$ for each sub-aperture in elevation, all signals will be combined together, as show in Figure 6.

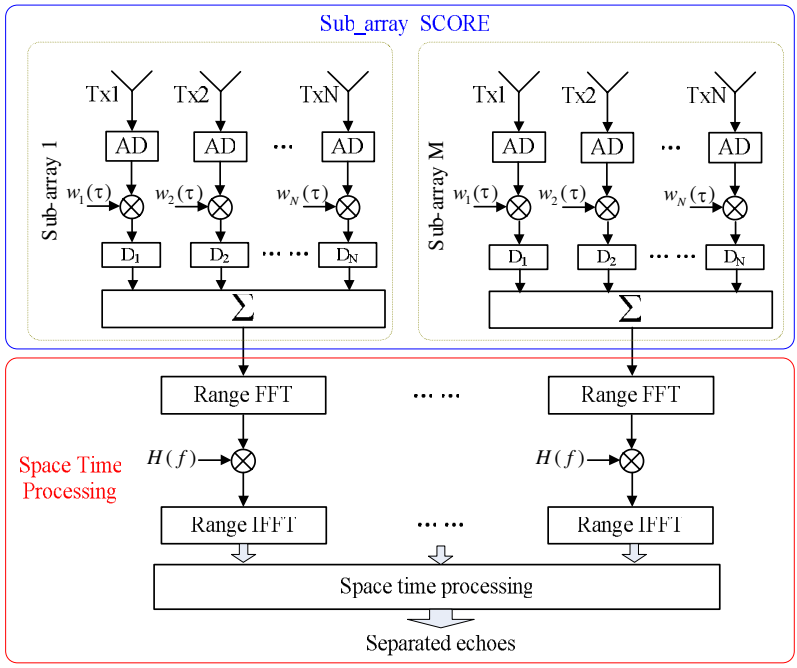


**Figure 6.** Block diagram of two step DBF operation in elevation in the proposed SAR system. The first step is implemented onboard via multiple sub-arrays in parallel, while the second step is performed on the ground.

As multiple sub-pulses are transmitted in a single PRI with the short time delay, echoes of different imaged targets corresponding to different sub-pulses may temporally overlap in the receiving window. However, they will arrive the receive antenna with different looking angles in elevation. Echoes from different subswaths seem to be more easily separated, as different subswaths are illuminated by different elevation beams. Furthermore, a careful transmit antenna by null steering is usually adopted to further reduce range ambiguous energy, as shown in Figure 4. Therefore, echoes from different subswath could be considered as well separated after the sub-array SCORE operation onboard.

### 3.2. Space Time Processing

Since sub-pulses with different polarizations in a single PRI are transmitted through the same transmit beam in elevation, all channels in elevation should combine together to form a narrower receive beam to separate echoes corresponding to sub-pulses with different polarizations. In the spaceborne SAR systems, the large pulse duration is usually adopted to achieve the desired SNR, signal energy of scattered targets will span in the whole pulse duration before range compression. Moreover, narrow receive beams of sub-array antennas are continuously steered during the whole receive time, and echoes of each point target will be received with a time variant antenna gain. It is hard to extract different angular diversities from the mixed signals. Therefore, range compression should be taken in each receive channel before combining all signals in elevation into one. After taking range compression, received signals by the multiple elevation channels can be expressed as matrix form by:

$$\mathbf{S}(\tau, t) = \mathbf{W}(\tau)\mathbf{Z}(\tau, t) \tag{12}$$

with

$$\mathbf{W}(\tau) = \begin{bmatrix} a_{1,1} & a_{1,2} & & a_{1,N_p} \\ a_{2,1} & a_{2,2} & \ddots & a_{2,N_p} \\ \vdots & \vdots & & \vdots \\ a_{M_r,1} & a_{M_r,2} & & a_{M_r,N_p} \end{bmatrix} \tag{13}$$

$$a_{m,i} = \exp\left[j\frac{2\pi}{\lambda}(m-1)d_r \sin\left(\theta_i(\tau)\right)\right]$$
$$m = 1, 2, \ldots, M_r \qquad i = 1, 2, \ldots, N_p \tag{14}$$

$$\mathbf{S}(\tau, t) = [s_1(\tau, t), \ldots, s_{M_r}(\tau, t)]^T \tag{15}$$

$$\mathbf{Z}(\tau, t) = [z_1(\tau, t), \ldots, z_{N_p}(\tau, t)]^T \tag{16}$$

where $t$ is the slow time, $\mathbf{S}(\tau, t)$ represents the echoes received by multiple elevation sub-array antennas in elevation, $\mathbf{Z}(\tau, t)$ indicates the echoes corresponding to sub-pulses with different polarizations, $[\cdot]^T$ is matrix transposed, $d_r$ is the height of sub-array antenna in elevation, $\theta_i(\tau)$ is the looking angle corresponding to the $i$th sub-pulse, $M_r$ is the number of the receive sub-array antennas in elevation, and $N_p$ is the number of the sub-pulses. Since $\theta_1 \neq \theta_2 \neq \ldots \neq \theta_{N_p}$ for each range sample time, $\mathbf{W}(\tau)$ is the matrix with column full rank, and its pseudo-inverse matrix $\mathbf{W}^+(\tau)$ can be calculated. Afterwards, $\mathbf{S}(\tau, t)$ can be obtained as follows:

$$\mathbf{Z}(\tau, t) = \mathbf{W}^+(\tau)\mathbf{S}(\tau, t) = \left(\mathbf{W}^H\mathbf{W}\right)^{-1}\mathbf{W}^H\mathbf{S}(\tau, t) \tag{17}$$

where $[\cdot]^H$ denotes the conjugate complex transposed. From (17), it can be seen that echoes corresponding to sub-pulses with different angular diversities will be separated.

Two point targets with the slant range 808.25 km (P2) and 800 km (P1) are assumed in the SAR imaging geometry, their echoes corresponding to different sub-pulses will be recorded as the same slant range as shown in Figure 7(a). To distinguish their different echoes, the reflectivity patterns $\sigma$ of the two point targets are with the relationship of $\sigma_1 : \sigma_2 = 2 : 1$. Figure 7(b) shows the simulation result after STP operation, and it clearly validates the proposed waveform diversity extraction approach.

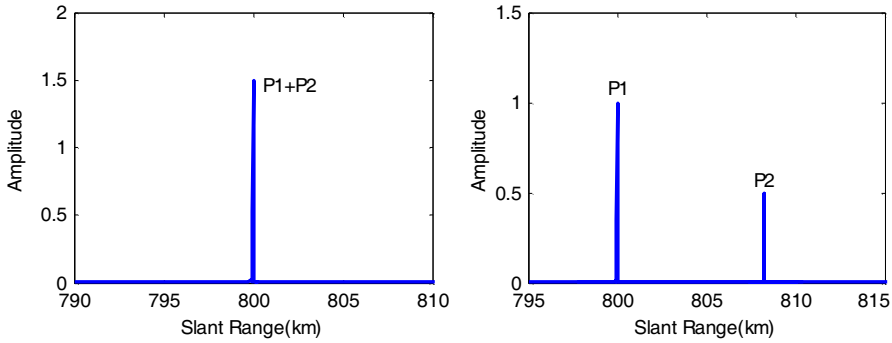


(a) Before extraction (b) After extraction

**Figure 7.** Echoes separation corresponding different subpulse.

### 3.3. Azimuth Preprocessing and Monostatic TOPS Mode Imaging

As the system pulse repetition frequency (PRF) selection in the spaceborne SAR systems mainly depends on the timing diagram selection and ambiguous energy suppression, challenges arise for the multi-channel SAR processing due to the non-uniform azimuth sampling. Moreover, the total Doppler spectrum is aliased due to progressive azimuth beam steering during the whole acquisition time in the TOPS mode Therefore, azimuth block division should be taken before multichannel azimuth data reconstruction as shown in Figure 8. Each azimuth sub-block data is with an individual squint angle, and then squinted multichannel data reconstruction is applied. To avoid the aliased Doppler spectrum, the size of each sub-block should be

$$T_{sub} \leq \frac{N_{az} \cdot \mathrm{PRF} - B_f}{k_{rot}} \tag{18}$$

where $N_{az}$ is the number of azimuth sub-apertures, $B_f$ is the azimuth beam bandwidth, and $k_{rot}$ is the Doppler varying rate in TOPS and given as follows [7]:

$$k_{rot} = \frac{2v_s\omega_r}{\lambda} \tag{19}$$

where $v_s$ is the velocity of SAR sensor, and $\omega_r$ is the azimuth beam rotation rate.

Up to now, multiple algorithms of azimuth multichannel data processing [26, 27] are proposed in recent years. After azimuth data recombination in the time domain, monostatic imaging algorithms in [7, 9] are adopted to process the residual raw data.

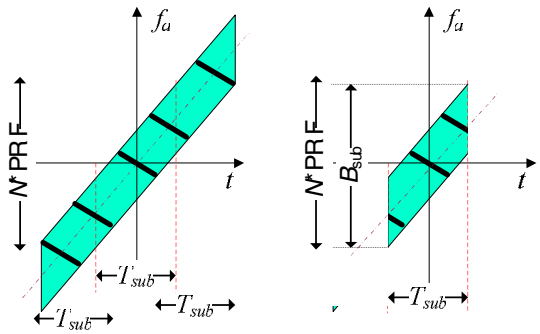


(a) The whole burst (b) The sub-block

**Figure 8.** Azimuth block division in the TOPS mode.

## 4. A SYSTEM DESIGN EXAMPLE

This section gives a MIMO-TOPS SAR system design example to demonstrate the applicability and potentials of the proposed operation for ultra-wide-swath full polarimetric imaging with a high geometric resolution. The selection of some parameters is introduced in detail. Afterwards, a performance analysis is carried out. All requirements and system constraints are listed in Table 1.

As nadir echoes can be reduced by a careful design of the transmit antenna pattern and DBF on receive in elevation with the null steering technique via a large receive antenna, the dark gray strips as shown in Figure 9 only indicate the direction signal reception. The incident angles vary from 19.3° to 47.7° to obtain about 400 km swath coverage, PRFs of 1190 Hz and 1110 Hz are chosen for two bursts, respectively.

With the maximum incident angle of 47.7° and the farthest slant range 890 km, Figure 10 shows the relation between the short time delay and the minimum antenna height. The total receive antenna with 4.8 m height, which consists of three sub-array apertures, is chosen, while two sub-pulses are transmitted in sequence with the time delay of 50 μs.

**Table 1.** Parameters of the system design example.

| Parameters | Value |
|---|---|
| Carrier frequency | 9.65 GHz |
| Sensor height (over earth) | 630 km |
| Sensor velocity | 7545 m/s |
| Incident angle range | 15–50° |
| Transmit sub-antenna size | $2.4\,\mathrm{m} * 0.4\,\mathrm{m}$ |
| Transmit sub-antenna T/R elements | $24 * 20$ |
| Peak Tx Power | 2880W |
| Receive antenna length | $2.4 * 6\,\mathrm{m}$ |
| System temperature | 300 K |
| Pulse duration | 40 μs |
| Pulse bandwidth | 150 MHz |
| Figure noise and Losses (2-way) | 5 dB |
| AASR | $< -20\,\mathrm{dB}$ |
| RASR | $< -25\,\mathrm{dB}$ |
| NESZ | $< -20\,\mathrm{dB}$ |

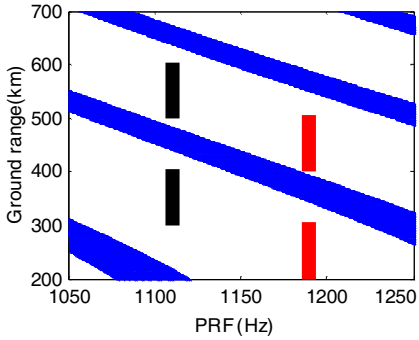


**Figure 9.** The timing diagram selection.

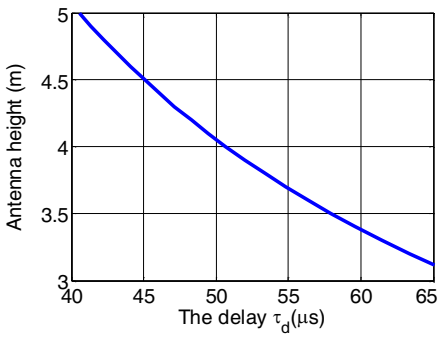


**Figure 10.** Receive antenna height selection.

To obtain the desired azimuth resolution $\rho_{az}$, the azimuth beam rotation rate $\omega_r$ can be approximately described as follows:

$$\omega_r = \frac{2\rho_{az}v_s - v_g L_a}{L_a R_c} \tag{20}$$

where $L_a$ is the transmit antenna length, $R_c$ is the slant range of imaging center in subswath. To obtain continuous TOPS-SAR image in each subswath, the timeline should be

$$(\omega_{r\_i} T_{B\_i} - \vartheta_0) R_{c\_i} + v_g T_{B\_i} = (1+\varepsilon) v_g \sum_{i}^{N} T_{B\_i} \tag{21}$$

where $T_{B\_i}$ is the burst duration for the burst $i$; $\vartheta_0$ is the angular interval to be exploited for azimuth data focusing; $\varepsilon$ is the ratio between the overlap coverage and the single burst effective imaging scene. This leads to a linear system of two equations in the unknown $T_{B\_i}$ in two-burst mode MIMO-TOPS SAR system. It should be noted that two subswaths are simultaneously illuminated during each burst and $R_{c\_i}$ is the slant range in the farther subswath for the burst $i$. Different subswaths with the same burst require different azimuth beam steering laws for the same azimuth resolution, but we chose the same azimuth beam steering law to reduce the system complexity. The designed results of the presented MIMO-TOPS mode are listed in Table 2.

Figure 11 shows the system performances range ambiguity to signal ratio (RASR) and Noise Equivalent Sigma Zero (NESZ) of the design system example. The RASR (solid line) varies from near to far range and it is even unsatisfied with the system requirement in the conventional SAR system. After the SCORE technique via the multiple sub-array antennas (dashed line) in elevation, range ambiguous energy will be seriously suppressed and the mean RASR

value in each subswath is reduced about 25 dB. In the SAR system, NESZ is a very important performance parameter which is a measure of the sensitivity of the system to areas of low radar backscatter. It represents the value of the backscatter coefficient corresponding to a signal-to-noise ratio (SNR), where SNR = 1. The NE$\sigma^0$ is a function of antenna gain which can be given as follows:

$$\mathrm{NE}\sigma^0 = \frac{256\pi^3 R^3 v_s \sin(\theta_i - \gamma) K B_r F L_{atm} L_{sys} L_{az}}{P_T G_T G_R \lambda^3 c\tau_p \cdot \mathrm{PRF}} \tag{22}$$

where $R$ is the average transmit and receive slant range, $\theta$ is the incident angle, $\gamma$ is the local slope angle, $K$ is the Boltzmann constant, $T$ is the radar receiver temperature, $B_r$ is the bandwidth of the radar pulse, $F$ is the noise figure, $L_{atm}$ and $L_{sys}$ represents the system losses and the atmospheric losses, respectively, $L_{az}$ is the azimuth losses. NE$\sigma^0$ in all subswath are below to $-22$ dB and satisfied with the system requirement listed in Table 2.

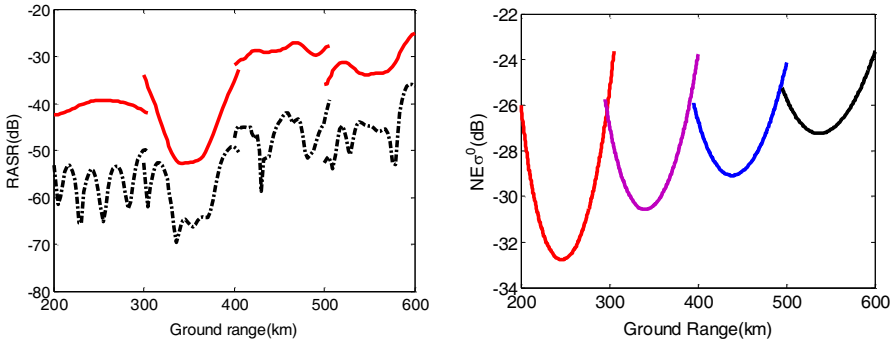


(a) RASR (b) NESZ

**Figure 11.** The presented MIMO-TOPS mode SAR system performances.

**Table 2.** Parameters of impulse response.

| | Swath 1 | Swath 2 | Swath 3 | Swath 4 |
|---|---|---|---|---|
| Incident angle (° ) | 19.3–28.3 | 27.5–35.5 | 35.1–42.1 | 41.7–47.7 |
| PRF (Hz) | 1190 | 1110 | 1190 | 1110 |
| Slant range (km) | 681.8 | 726.6 | 783.9 | 850.2 |
| Swath depth (km) | 105 | 105 | 105 | 100 |
| Burst length (s) | 2.09 | 2.13 | 2.09 | 2.13 |
| Rotation rate (°/s) | 0.88 | 0.81 | 0.88 | 0.81 |

## 5. CONCLUSION

An innovative MIMO-TOPS mode for high resolution ultra wide swath full polarimetric imaging is introduced in this paper. Sub-pulses with different polarizations illuminating the same subswath are transmitted by different sub-aperture antennas in azimuth with a short time delay. Mapping of multiple subswaths during each burst and the DPCA technique are adopted to improve the impaired TOPS mode azimuth resolution. The temporal phenomenon of echoes overlap at receivers is resolved by the modified DBF on receive approach in elevation, which takes advantage of the SCORE technique via multiple sub-array antennas in parallel onboard and space time processing on the ground to reduce the major drawbacks of the existing DBF on receive approaches in elevation. A design example of the proposed MIMO-TOPS full polarimetric SAR system with the imaging capacity of 400 km swath width and an azimuth resolution of 3 m is given to demonstrate the potential for future spaceborne SAR missons.

## ACKNOWLEDGMENT

This work was supported by the Department of Spaceborne Microwave Remote Sensing, Institute of Electronics, Chinese Academy of Sciences (IECAS).

## REFERENCES

1. Chan, Y. K. and V. C. Koo, "An introduction to synthetic aperture radar (SAR)," *Progress In Electromagnetics Research B*, Vol. 2, 27–60, 2008.
2. Angulo, L. D., S. G. Garcia, M. Fernandez Pantoja, C. Cobos Sanchez, and R. Gomez Martin, "Improving the SAR distribution in petri-dish cell cultures," *Journal of Electromagnetic Waves and Applications*, Vol. 24, No. 5–6, 815–826, 2010.
3. Lim, S. H., J.-H. Han, S.-Y. Kim, and N.-H. Myung, "Azimuth beam pattern synthesis for airborne SAR system optimization," *Progress In Electromagneitcs Research*, Vol. 106, 295–309, 2010.
4. Chan, Y. K. and S. Y. Lim, "Synthetic aperture radar (SAR) signal generation," *Progress In Electromagnetics Research B*, Vol. 1, 269–290, 2008.
5. Li, C. and D.-Y. Zhu, "A residue-pairing algorithm for insar phase unwrapping," *Progress In Electromagnetics Research*, Vol. 95, 341–354, 2009.

6. Sun, J., S. Mao, G. Wang, and W. Hong, "Extended exact transfer function algorithm for bistatic SAR of translational invariant case," *Progress In Electromagnetics Research*, Vol. 99, 89–108, 2009.
7. Zan, F. D. and A. M. Guarnieri, "TOPSAR: Terrain observation by progressive scans," *IEEE Trans. Geosci. Remote Sens.*, Vol. 44, No. 9, 2352–2360, Sep. 2006.
8. Meta, A., J. Mittermayer, P. Prats, R. Scheiber, and U. Steinbrecher, "TOPS imaging with TerraSAR-X: Mode design and perfomance analysis," *IEEE Trans. Geosci. Remote Sens.*, Vol. 48, No. 2, 759–769, Feb. 2010.
9. Prats, P., R. Scheiber, J. Mittermayer, A. Meta, and A. Moreira, "Processing of sliding spotlight and TOPS SAR data using baseband azimuth scaling," *IEEE Trans. Geosci. Remote Sens.*, Vol. 48, No. 2, 770–780, Feb. 2010.
10. Chua, M. Y. and V. C. Koo, "FPGA-based chirp generator for high resolution UAV SAR," *Progress In Electromagnetics Research*, Vol. 99, 71–88, 2009.
11. Sun, J., S. Mao, G. Wang, and W. Hong, "Polar format algorithm for spotlight bistatic SAR with arbitrary geometry configuration," *Progress In Electromagnetics Research*, Vol. 103, 323–338, 2010.
12. Krieger, G., N. Gebert, M. Younis, F. Bordoni, A. Patyuchenko, and A. Moreira, "Advanced concepts for ultra-wide-swath SAR imaging with high azimuth resolution," *Proc. EUSAR*, Friedrichshafen, Germany, 2008.
13. Gebert, N., G. Krieger, and A. Moreira, "Multi-channel ScanSAR for high-resolution ultra-wide-swath imaging," *Proc. EUSAR*, Friedrichshafen, Germany, 2008.
14. Gebert, N., G. Krieger, and A. Moreira, "Multichannel azimuth processing in ScanSAR and TOPS mode operation," *IEEE Trans. Geosci. Remote Sens.*, Vol. 48, No. 7, 2994–3008, Jul. 2010.
15. Wei, S.-J., X.-L. Zhang, J. Shi, and G. Xiang, "Sparse reconstruction for SAR imaging based on compressed sensing," *Progress In Electromagnetics Research*, Vol. 109, 63–81, 2010.
16. Zhao, Y. W., M. Zhang, and H. Cheng, "An efficient ocean SAR raw signal simulation by employing fast Fourier transform," *Journal of Electromagnetic Waves and Applications*, Vol. 24, No. 16, 2273–2284, 2010.
17. Mao, X., D.-Y. Zhu, and Z.-D. Zhu, "Signatures of moving target in polar format spotlight SAR image," *Progress In Electromagnetics Research*, Vol. 92, 47–64, 2009.

18. Zhang, Y.-D., L. Wu, and G. Wei, "A new classifier for polarimetric SAR images," *Progress In Electromagnetics Research*, Vol. 94, 83–104, 2009.
19. Teng, H. T., H.-T. Ewe, and S. L. Tan, "Multifractal dimension and its geometrical terrain properties for classification of multi-band multi-polarized SAR image," *Progress In Electromagnetics Research*, Vol. 104, 221–237, 2010.
20. Jin, Y.-Q., "Polarimetric scattering modeling and information retrieval of SAR remote sensing — A review of fdu work," *Progress In Electromagnetics Research*, Vol. 104, 333–384, 2010.
21. Krieger, G., N. Gebert, and A. Moreira, "Multidimensional waveform encoding for synthetic aperture radar remote sensing," *Proc. International Conference on Radar Systems (RADAR)*, Edinburgh, UK, 2007.
22. Krieger, G., N. Gebert, and A. Moreira, "Multidimensional waveform encoding: A new digital beamforming technique for synthetic aperture radar remote sensing," *IEEE Trans. Geosci. Remote Sens.*, Vol. 46, No. 1, 31–46, Jan. 2008.
23. Xu, W. and Y. Deng, "Multi-channel SAR system with reflector antenna for high-resolution wide-swath imaging," *IEEE Antenna and Wireless Propa. Lett.,* Vol. 9, 1123–1126, Dec. 2010.
24. Junghyo, K., O. Alicja, and W. Werner, "Investigation of MIMO SAR for interferometry," *Proc. EUSAR*, Friedrichshafen, Germany, 2008.
25. Suess, M., B. Grafmueller, and R. Zahn, "A novel high resolution, wide swath SAR system," *Proc. IGARSS*, Sydney, Australia, 2001.
26. Krieger, G., N. Gebert, and A. Moreira, "Unambiguous SAR signal reconstruction from nonuniform displaced phase center sampling," *IEEE Geosci. Remote Sens. Lett.*, Vol. 1, No. 4, 260–264, Oct. 2004.
27. Gebert, N., G. Krieger, and A. Moreira, "Digital beamforming on receive: Techniques and optimization strategies for high-resolution wide-swath SAR imaging," *IEEE Trans. Aerosp. Electron. Syst.*, Vol. 54, No. 2, 564–592, Apr. 2009.